Journal of Solid State Chemistry 183 (2010) 105–113

Contents lists available at ScienceDirect

Journal of Solid State Chemistry

journal homepage: www.elsevier.com/locate/jssc

Low temperature structural transformation in $T[Ni(CN)_4]\cdot x$pyz with $x=1,2$; T=Mn,Co,Ni,Zn,Cd; pyz=pyrazine

J. Rodríguez-Hernández [a,b], A.A. Lemus-Santana [c], J. Ortiz-López [d], S. Jiménez-Sandoval [e], E. Reguera [b,*,1]

[a] Centro de Investigación en Ciencia Aplicada y Tecnología Avanzada del IPN, Unidad Legaría, México, D.F. Mexico
[b] Instituto de Ciencia y Tecnología de Materiales, Universidad de La Habana, Cuba
[c] Departamento de Polímeros, Instituto de Investigaciones en Materiales, Universidad Nacional Autónoma de México, México, D.F. Mexico
[d] Escuela Superior de Física y Matemáticas del IPN, UP "ALM", Col. Lindavista, México, D.F., Mexico
[e] Centro de Investigación y Estudios Avanzados del IPN, Unidad Querétaro, Querétaro, Mexico

ARTICLE INFO

Article history:
Received 3 June 2009
Received in revised form
18 September 2009
Accepted 2 November 2009
Available online 10 November 2009

Keywords:
Crystal chemistry
Low temperature structure
Layered compounds
Pillared solids

ABSTRACT

The materials under study are pillared solids $T[Ni(CN)_4]\cdot x$pyz with one and two ($x=1,2$) pyrazine (pyz) molecules and where T=Mn, Co, Ni, Zn, Cd. Stimulated by their structural features and potential role as prototype of porous solids for hydrogen storage, the structural stability under cryogenic conditions for this series of pillared solids was studied. At low temperature, in the 100–200 K range, the occurrence of a reversible structural transformation was found. For T=Mn, Co, Zn, Cd, with $x=2$, the structural transformation was observed to occur around 185 K, and the low temperature phase crystallizes with a monoclinic unit cell (space group *Pc*). This structure change results from certain charge redistribution on cooling within the involved ligands. For T=Ni with $x=1$, both the low and high temperature phases crystallize with unit cells of tetragonal symmetry, within the same space group but with a different unit cell volume. In this case the structure change is observed around 120 K. Above that temperature the rotational states for the pyrazine molecule are thermally excited and all the pyrazine molecules in the structure become equivalent. Under this condition the material structure is described using a smaller structural unit. The structural study using X-ray powder diffraction data was complemented with calorimetric and Raman spectroscopy measurements. For the low temperature phases the crystal structures were solved from Patterson methods and then refined using the Rietveld method.

1. Introduction

Tridimensional (3D) solids prepared by incorporation of pillars (L) in layered compounds (2D) form an interesting class of porous materials. Within pillared 2D solids divalent transition metal (T) salts of the tetracyanometallate complex anion, $T[M(CN)_4]$, with M=Ni, Pd, Pt, are particularly attractive because allow the incorporation of neutral pillar molecules between metal center on neighboring layers. This family of pillared coordination polymers is receiving certain attention as prototype of porous materials for hydrogen storage [1,2] and also for studies related with their spin crossover behavior [3–10]. Since both the hydrogen storage and spin transition studies usually occur at low temperatures, the interpretation of the obtained experimental results must be accompanied of the availability of information on the material structural stability under cryogenic conditions. To the best of our knowledge, for the series of materials herein studied, such information is not available.

For T=Co, Ni, the incorporation of pyrazine (pyz), 4,4′-bipyridine and 4,4′-dipyridylacetylene as pillar groups between T metal centers on neighboring layers has been reported [1,2]. The obtained materials crystallize with a tetragonal unit cell ($P4/m$ space group) creating a 3D porous framework formed by interconnected rectangular channels of the same width but of different height; this last feature due to the length of the used pillar molecule. These 3D frameworks of tailored channel size and shape have been used in studies oriented to shed light on the role of the pore dimension and geometry on the hydrogen storage in porous solids [2]. Related to the ability of the iron (2+) atom to form both high and low spin complexes, the series $Fe_{1-x}T_x[M(CN)_4]\cdot$pyz where T=Co, Ni and M=Ni, Pd, Pt, has been intensively studied in order to understand the nature of their low temperature spin-crossover behavior, particularly the pronounced hysteresis loop that is observed [4–8]. In a recent paper, we have reported the preparation and characterization of $T[Ni(CN)_4]\cdot 2$pyz frameworks with T=Mn, Zn and Cd where the

* Corresponding author.
E-mail address: ereguera@yahoo.com (E. Reguera).
[1] On leave from Instituto de Ciencia y Tecnología de Materiales, Universidad de La Habana, Cuba.

0022-4596/$ - see front matter © 2009 Elsevier Inc. All rights reserved.
doi:10.1016/j.jssc.2009.11.004

pillar ligand (pyz) is found forming bridges with both Ni and *T* metal centers on neighboring layers but with a non-vertical alternating crossed configuration [11]. These last three compositions crystallize with an orthorhombic unit cell (*Pnc*2 space group). The channels for the resulting porous solids are of insufficient size to be considered of interest for H_2 storage because the absorbate diffusion rate is very low [11]. In this contribution, the low temperature structural stability of $Co[Ni(CN)_4]\cdot pyz$, $Ni[Ni(CN)_4]\cdot pyz$ and $T[Ni(CN)_4]\cdot 2pyz$ with *T*=Mn, Co, Zn, Cd, is discussed from high-resolution X-ray diffraction (HR-XRD), Raman spectra, and calorimetric data. These compositions are representative of the two structures (tetragonal *P*4/*m* and orthorhombic *Pnc*2) found for divalent transition metals tetracyanonickellates pillared with pyrazine.

2. Experimental section

The preparative route to obtain samples of $T[Ni(CN)_4]\cdot 2pyz$ with *T*=Mn, Co, Zn, Cd has already been reported [11] and it is summarized as follow: the layered solid $T[Ni(CN)_4]$ is obtained when diluted aqueous solutions of $[Ni(CN)_4]^{2-}$ (from $K_2[Ni(CN)_4]$) and of T^{2+} are mixed followed by separation of the formed precipitate by centrifugation; then the layers are separated (detached) in a 0.3 M solution of citric acid followed by addition, drop by drop, of a diluted solution of ammonium hydroxide solution (20% v/v) until the precipitate disappearance, when a pyrazine (0.07 M) solution is added under stirring. The formation of the pillared solid is achieved when the solution pH is adjusted to be in the 4–5 range, by adding the appropriate amount of diluted citric acid. Under the same reaction conditions, for Co and Ni the single pyrazine compounds (tetragonal phase), $Co[Ni(CN)_4]\cdot pyz$, $Ni[Ni(CN)_4]\cdot pyz$, are obtained. The nature of the resulting solids as pillared compounds was established from energy-dispersed spectroscopy (EDS), infrared (IR), Raman, UV–Vis, thermogravimetric (TG) and XRD data.

The HR-XRD powder patterns were collected at the XPD-10B beamline at the LNLS synchrotron radiation facility (Campinas, Brazil), at room conditions and under vacuum (10^{-6} mm Hg) in the 12–300 K temperature range on cooling and then on heating. The wavelength used was 1.549950 Å (7.9998 keV). The experimental details are summarized in Table 1. The crystal structures were solved *ab initio* by Patterson methods using the program SHELXS [12] from extracted intensities according to the Le Bail method [13]. The structural refinement from these XRD powder patterns was performed with the Rietveld method using the FullProf program [14] and pseudo-Voigt peak shape function. Peak profiles were calculated within 10 times the full width at half maximum (FWHM). The background was modeled by a third-order polynomial. The interatomic C–N and Ni–C distances were constrained to take values within certain limits considering results from the structural study of the parent high temperature phases [11]. The materials framework 3D illustration and the available free spaces and slit size were calculated from the refined crystal structure.

Heat capacity at constant pressure C_p was measured with an AC calorimeter (ULVAC/Sinku-Riko, model ACC-VL-1). Samples were prepared from pellets of compressed powders with 0.2–0.3 mm thickness and no more than 3×3 mm^2 in area. C_p measurements were performed on cooling from room temperature (RT) down to 77 K without any control, and on heating from 77 K to RT at a controlled constant rate of 1 K/min. High purity He gas (99.999%) at low pressure (10 Torr) acted as thermal bath and its temperature was monitored with a Pt sensor. The samples were thermally excited on one face with light from a halogen lamp chopped at a frequency of 3 Hz, while its AC temperature T_{AC} was measured on the opposite face with a very thin chromel-constantan thermoucouple connected to a lock-in amplifier. The excitation frequency of 3 Hz is chosen so that C_p becomes inversely proportional to the measured T_{AC}.

The Raman spectra were obtained in a Dilor Labram micro spectrometer at room temperature and 80 K using the 514.5 nm excitation line of an Ar+ laser. The laser beam was focused on the sample surface with a 50× microscope objective. Special care was taken to avoid sample modifications due to laser heating effects. The signal was analyzed with the help of a 256× 1024-pixel CCD detector. For the low temperature measurements the samples were mounted on the cold stage of an Oxford Microstat N.

3. Results and discussion

3.1. Characterization of the solids to be studied

The structural characterization and related properties of $T[Ni(CN)_4]\cdot 2pyz$ with *T*=Mn, Zn, Cd have already been discussed [11] and here only a summary of their features is provided. In the course of this study for *T*=Co the formed solid was found to be iso-structural with these three compounds. This result indicates that for Co the two phases, orthorhombic ($T[Ni(CN)_4]\cdot 2pyz$) and tetragonal ($T[Ni(CN)_4]\cdot pyz$), are possible to be formed. The unit cell parameters for these four orthorhombic (*Pnc*2 space group) solids at room temperature are available from the Supplementary information file. In the orthorhombic phase all the pyrazine molecules are forming bridges between Ni and *T* metals in the interlayers region, Ni–pyrazine–*T*. Along the **c** axis, the pyrazine molecules are found stacked according to a crossed configuration. In the 3D structure of $T[Ni(CN)_4]\cdot 2pyz$, the layers of $T[Ni(CN)_4]$ appear as rippled sheets related to deviation for the N–*T*–N chains from the linearity, $\angle$N–*T*–N=174.5°, quite different from the structural feature of a layered structure, $T[Ni(CN)_4]$, where $\angle$N–*T*–N ~180°. Such rippled sheets conformation for the pillared solids is ascribed to a different bonding interaction of the pyrazine molecule with *T* and Ni atoms and also to the possibility of certain flexibility around the *T*–NC bond within the layer. In this structure the two metal centers are found with a

Table 1
Experimental details for the HR-XRD data collection.

77 K	ZnNi2pyz	MnNi2pyz	CdNi2pyz	CoNi2pyz	NiNipyz
Data collection					
Diffractometer	D10B-XPD powder X-ray diffraction beamline, at the Brazilian Synchrotron Light Laboratory (LNLS)				
Monochromator	Analyzer crystal: Ge(111)				
Wavelength (Å)	1.54995 Å				
2θ range (deg)	10.0–80.0	10.0–75.0	10.0–70.0	10.0–70.0	10.0–70.0
Step size (deg)	0.008	0.02	0.01	0.015	0.015
Time per step (s)	1	2	1	2	1

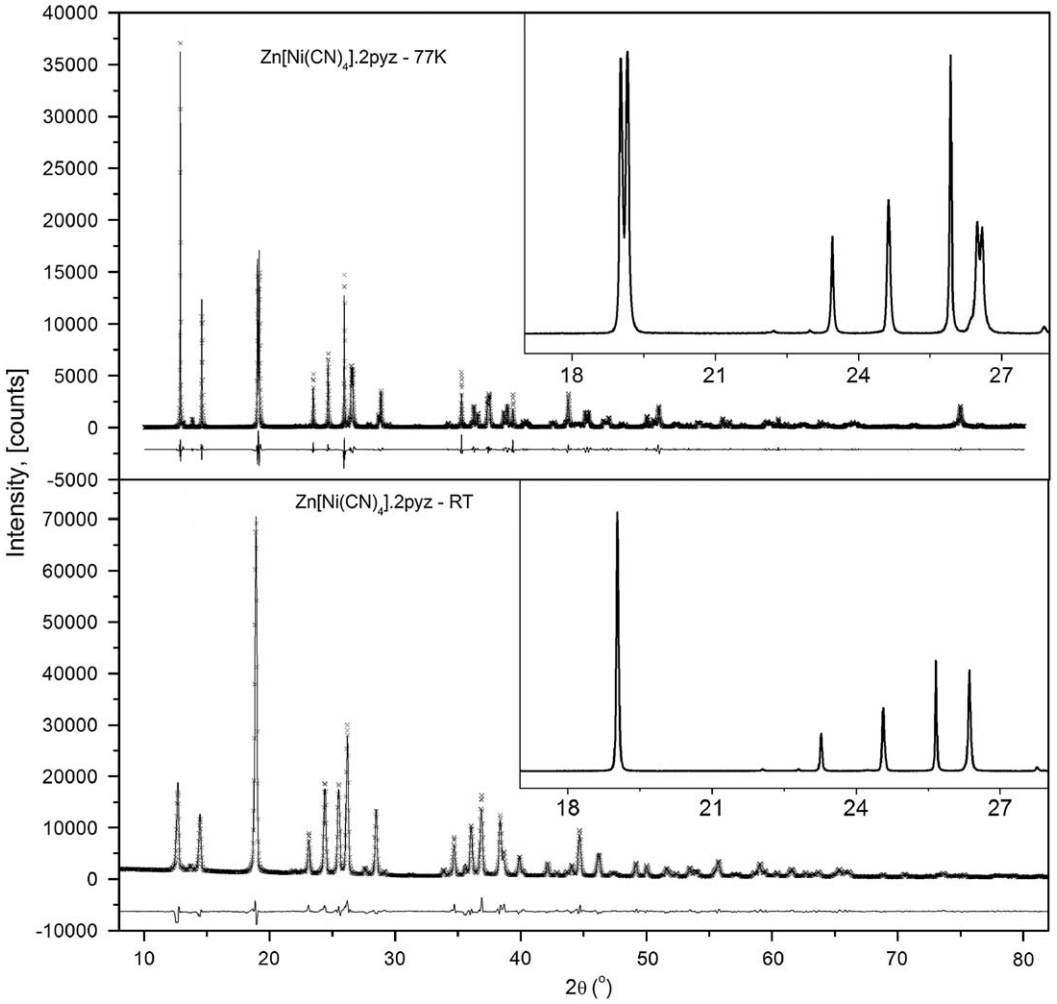

Fig. 1. XRD powder patterns for $Zn[Ni(CN)_4]\cdot 2pyz$ at room temperature and at 77 K. The insets illustrate the splitting of some diffraction peaks, indicating the occurrence of a reversible structural transition on cooling.

pseudo-octahedral coordination, $NiC_4(N_2)_{pyz}$ and $T(N_4)_{CN}(N_2)_{pyz}$. The presence of pyrazine bridges linking both Ni and *T* metals leads to the formation of a relatively compact framework, where the available free spaces can only be used for the adsorption of small molecules like H_2 but with a low diffusion rate. These structural features are supported by magnetic measurements, and IR, Raman, UV–vis, TG, XRD and adsorption data [11].

The crystal structures for $Co[Ni(CN)_4]\cdot pyz$ and $Ni[Ni(CN)_4]\cdot pyz$ have been reported with a tetragonal unit cell (*P*4/*m* space group) [1]. Our results coincide with the reported structure where pyrazine molecule appears rotating around its vertical axis (see Supplementary information). This is an expected result since there is no preferential orientation of the plane ring or a restriction to the free rotation along the N–N coordination axis, and at room temperature the thermal energy is sufficient to exciting the rotational states. The calculated unit cell parameters at room temperature for this pillared solid are available from Supplementary information. In the structure of these tetragonal phases the pyrazine molecule forms vertical bridges through a coordination bond with the *T* metal centers found at neighboring layers but not with Ni atom coordinated at C end of the CN group. This leads to the formation of a 3D porous framework where channels of rectangular cross section of *c.a.* 4×10 Å remain interconnected. In the as-synthesized material these free spaces are occupied by water molecules, which can be removed by moderate heating under vacuum.

3.2. Low temperature structural transformation

The HR-XRD powder patterns for $Zn[Ni(CN)_4]\cdot 2pyz$ and $Ni[Ni(CN)_4]\cdot pyz$ at room temperature and 77 K, both under vacuum, are shown in Figs. 1 and 2, respectively. For the two structures (orthorhombic and tetragonal) the occurrence of a low temperature structural transformation is observed. For the orthorhombic phase the structural transition is detected as splitting for the main diffraction peaks (Fig. 1), while for the tetragonal one a series of new weak peaks appears (Fig. 2). The low temperature XRD pattern recorded for Zn corresponds to a monoclinic unit cell (*Pc* space group) with cell parameters slightly different from those corresponding to the high temperature structure (Table 2). For Ni the low temperature phase also crystallizes with a tetragonal unit cell and in the same space group (*P*4/*m*) (Table 2). However, that symmetry is conditioned to the inclusion of two formula units ($Z=2$) within the unit cell instead of $Z=1$ for the original structure, with the corresponding changes for the structural motif and cell parameters: $a'=b'=a\sqrt{2}$, $c'=c$ (see Supplementary information). XRD powder patterns were

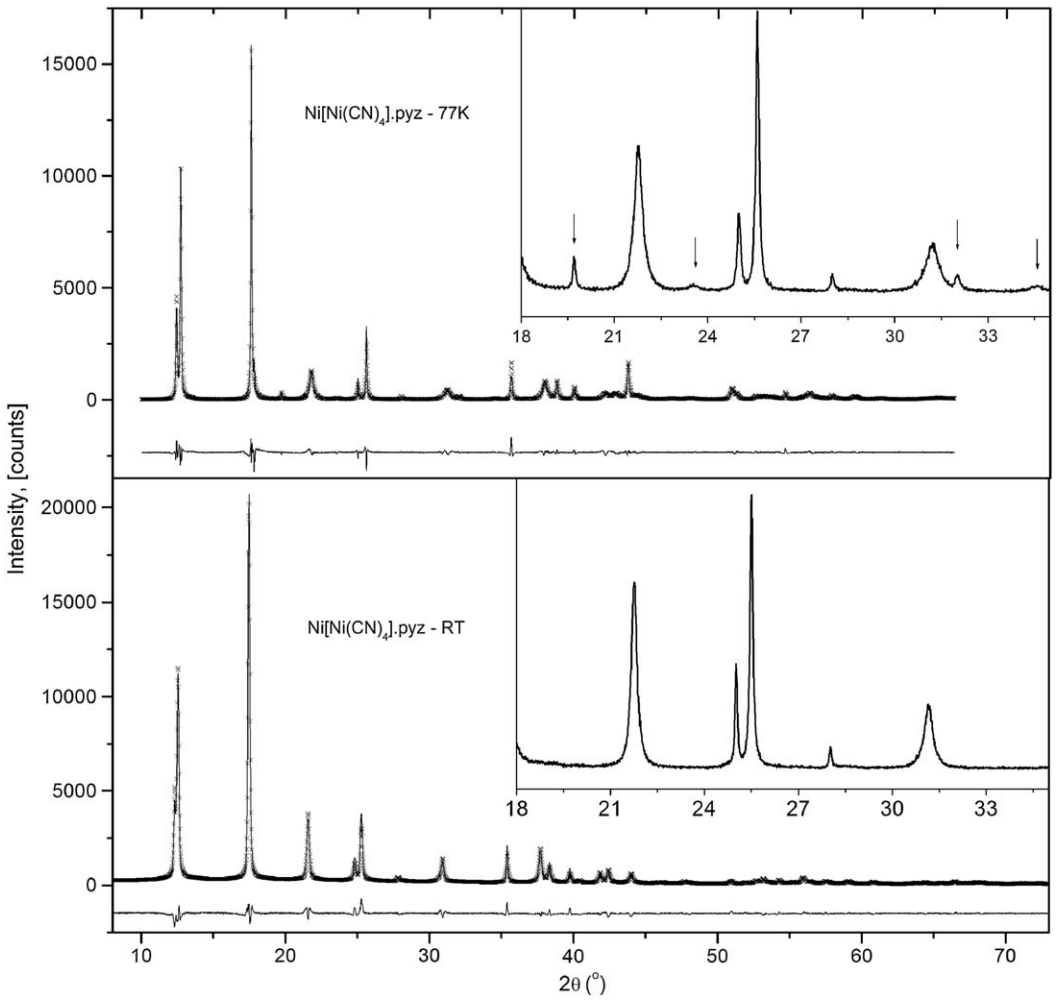

Fig. 2. XRD powder patterns for $Ni[Ni(CN)_4]\cdot pyz$ at room temperature (RT) and at 77 K. The insets illustrate the appearance of new diffraction peaks in the 77 K pattern, indicating the occurrence of a reversible structural transition on cooling.

Table 2
Unit cell parameters for the low temperature phases.

77 K	ZnNi2pyz	MnNi2pyz	CdNi2pyz	CoNi2pyz	NiNipyz
Unit cell					
Space group	*Pc*	*Pc*	*Pc*	*Pc*	*P4/m*
Parameter (Å)	a=6.7997(1)	a=6.7694(3)	a=6.9380(2)	a=6.7921(3)	a=10.149(5)
	b=13.8178(1)	b=13.8198(4)	b=14.0441(2)	b=13.8302(5)	b=10.149(5)
	c=7.2664 (1)	c=7.2447(2)	c=7.4554(2)	c=7.2662(3)	c=7.028(5)
	β=90.46(1)	β=90.3(1)	β=91.01(1)	β=90.35(3)	
V (Å^3)	682.7(1)	677.7(4)	726.3(1)	683.1(2)	723.8(2)
Z	2	2	2	2	2
Refinement					
Nr. of contributing reflections	411	346	313	293	153
Nr. of distance constraints	8	8	8	8	4
Nr. of refined parameters					
Structural parameters	70	70	70	70	13
Profile parameters	14	14	14	14	11
Rexp	5.74	6.20	7.02	7.35	7.63
Rwp	11.2	10.8	12.6	12.4	13.1
RB	11.1	9.5	11.5	10.2	10.5
S	1.95	1.74	1.79	1.69	1.72

also recorded at 12 K and no other structure change was detected. For $T[Ni(CN)_4]\cdot 2pyz$ the structural change involves a slight reduction for the unit cell volume per formula unit, which amounts (in %): 1.37 (Mn), Co(1.31), 1.74 (Zn) and 1.69 (Cd).

In order to identify the temperature value for the structural change, XRD powder patterns at different temperatures in the 77–200 K range were recorded. For the orthorhombic phase that temperature is in the 180–200 K range, while for Ni it is around 120 K.

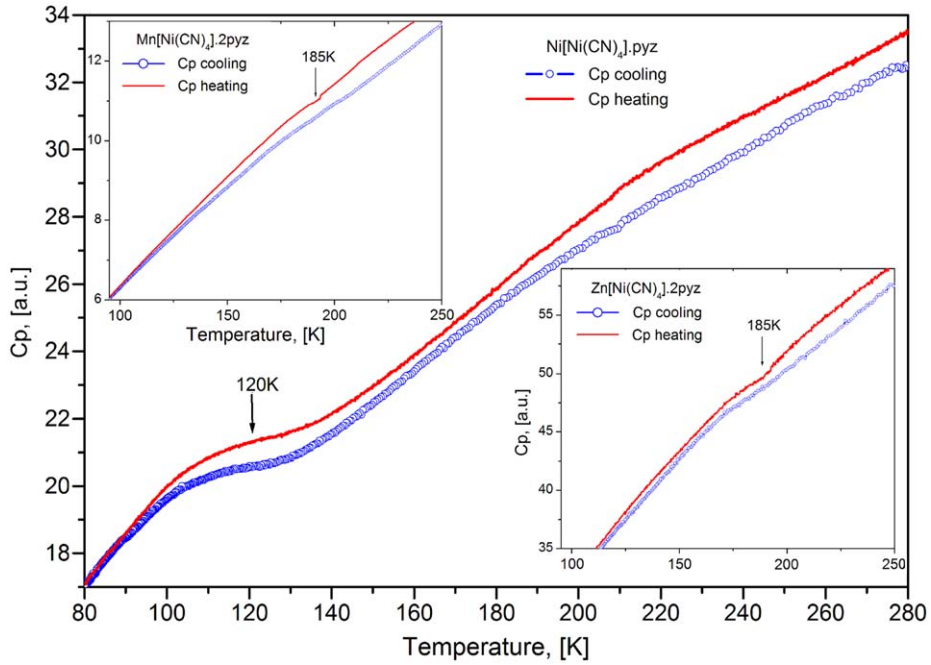

Fig. 3. C_p versus temperature curves for $Ni[Ni(CN)_4]\cdot pyz$, $Mn[Ni(CN)_4]\cdot 2pyz$, $Zn[Ni(CN)_4]\cdot 2pyz$. For Ni the inflection related to the structural transformation is particularly pronounced and the change in the curve slope below and above the transition temperature is quite different.

Table 3
Atomic positions and temperature (Biso) and occupation (Occ) factors for the refined crystal structures of $Zn[Ni(CN)_4]\cdot 2pyz$ and $Ni[Ni(CN)_4]\cdot pyz$.

Composition	Site	*x*	*y*	*z*	Biso	Occ
$Zn[Ni(CN)_4]\cdot 2pyz$-77K						
Zn	2*a*	0.159(2)	0.246(1)	0.333(2)	1.94(2)	1
Ni	2*a*	0.677(1)	0.251(2)	−0.152(1)	2.04(2)	1
$C1_{CN}$	2*a*	0.468(3)	0.242(4)	0.026(2)	2.5(1)	1
$N1_{CN}$	2*a*	0.344(3)	0.236(4)	0.131(2)	2.5(1)	1
$C2_{CN}$	2*a*	0.491(2)	0.223(3)	−0.345(3)	2.5(1)	1
$N2_{CN}$	2*a*	0.381(4)	0.206(3)	−0.461(3)	2.5(1)	1
$C3_{CN}$	2*a*	0.869(1)	0.275(2)	0.041(2)	2.5(1)	1
$N3_{CN}$	2*a*	0.982(3)	0.288(4)	0.154(3)	2.5(1)	1
$C4_{CN}$	2*a*	0.867(4)	0.262(3)	−0.346(4)	2.5(1)	1
$N4_{CN}$	2*a*	0.979(4)	0.269(5)	−0.461(3)	2.5(1)	1
$N5_{pyz}$	2*a*	0.313(5)	0.404(3)	0.379(2)	3.1(2)	1
$N6_{pyz}$	2*a*	0.481(3)	0.574(4)	0.413(2)	3.1(2)	1
$C5_{pyz}$	2*a*	0.183(2)	0.477(2)	0.414(3)	3.1(2)	1
$C6_{pyz}$	2*a*	0.522(4)	0.407(3)	0.394(2)	3.1(2)	1
$C7_{pyz}$	2*a*	0.287(4)	0.567(5)	0.381(3)	3.1(2)	1
$C8_{pyz}$	2*a*	0.593(2)	0.507(4)	0.423(4)	3.1(2)	1
$N9_{pyz}$	2*a*	0.019(2)	0.096(3)	0.375(3)	3.1(2)	1
$N10_{pyz}$	2*a*	−0.148(3)	−0.074(3)	0.413(3)	3.1(2)	1
$C9_{pyz}$	2*a*	0.149(2)	0.023(3)	0.414(2)	3.1(2)	1
$C10_{pyz}$	2*a*	−0.189(4)	0.093(4)	0.390(2)	3.1(2)	1
$C11_{pyz}$	2*a*	0.045(5)	−0.067(3)	0.381(4)	3.1(2)	1
$C12_{pyz}$	2*a*	−0.261(6)	−0.001(1)	0.423(3)	3.1(2)	1
$Ni[Ni(CN)_4]\cdot pyz$-77K						
$Ni2_C$	1*a*	0	0	0	1.91(2)	1
$Ni1_C$	1*c*	0.5	0.5	0	1.91(2)	1
$Ni3_N$	2*e*	0.5	0	0	1.87(3)	1
$C1_{CN}$	4*j*	0.5	0.303(2)	0	2.1(5)	1
$N1_{CN}$	4*j*	0.5	0.197(3)	0	2.1(5)	1
$C2_{CN}$	4*j*	0	0.192(6)	0	2.1(5)	1
$N2_{CN}$	4*j*	0	0.314(3)	0	2.1(5)	1
$N3_{pyz}$	4*i*	0.5	0	0.294(4)	2.6(6)	1
$C3_{pyz}$	8*l*	0.484(1)	0.137(3)	0.412(4)	2.6(6)	1

Table 4
Distances (in Å) and bond angles (in deg) for the refined structures.

Bond distances (Å)	Angle (deg)	
$Zn[Ni(CN)_4]\cdot 2pyz$-77K		
$Ni–C1_{CN}$=1.929(2)	Ni–C1–N1=179.8(4)	Zn–N1–C1=169.1(5)
$Ni–C2_{CN}$=1.930(2)	Ni–C2–N2=179.5(4)	Zn–N2–C2=153.3(5)
$Ni–C3_{CN}$=1.929(2)	Ni–C3–N3=179.9(5)	Zn–N3–C3=152.7(4)
$Ni–C4_{CN}$=1.929(2)	Ni–C4–N4=179.9(4)	Zn–N4–C4=165.5(4)
$Zn–N1_{CN}$=1.946(3)	Ni–N6–C8=111.9(4)	Zn–N5–C5=114.1(3)
$Zn–N2_{CN}$=2.188(3)	Ni–N6–C7=120.2(3)	Zn–N5–C6=117.5(4)
$Zn–N3_{CN}$=1.858(2)	Ni–N10–C11=117.2(5)	Zn–N9–C9=115.1(3)
$Zn–N4_{CN}$=1.967(3)	Ni–N10–C12=117.0(4)	Zn–N9–C10=116.7(4)
$Ni[Ni(CN)_4]\cdot pyz$-77K		
$Ni1–C1_{CN}$=1.982(2)		
$Ni2–C2_{CN}$=1.981(2)	Ni3–N3–C3=119.9(2)	
$Ni3–N2_{NC}$=1.915(2)	C3–N3–C3=120.2(2)	
$Ni3–N1_{NC}$=1.937(3)		
$Ni3–N3_{pyz}$=2.060(3)		

The inflection in the C_p versus temperature curves (Fig. 3) on heating indicates that at certain temperature the material consumes energy (endothermic effect) in a physical process different to the sample heating. The inverse behavior is observed for the recorded curves on cooling; at approximately the same temperature region, the material liberates energy (exothermic effect). The energy consumption or release at approximately the same temperature corresponds to the occurrence of a reversible process and agrees with above mentioned structural behavior, observed at approximately the same temperature values. From that inflection, the transformation temperature was estimated to be 185 K for the room temperature orthorhombic phase and 120 K for the tetragonal one (Fig. 3). For the tetragonal phase the change in the C_p value is particularly pronounced, accompanied also of a large variation for the curve slope below and above the temperature of transformation (Fig. 3), features that are not observed for the orthorhombic structure. That slope change suggests that for the tetragonal phase not only a structural change occurs but also a thermally activated process is contributing. Such process is the activation for the rotational states of the pyrazine molecule (discussed below). For the

tetragonal phase also a slight slope variation about 210 K was also observed, but not related to a structural change, according to the recorded XRD powder patterns.

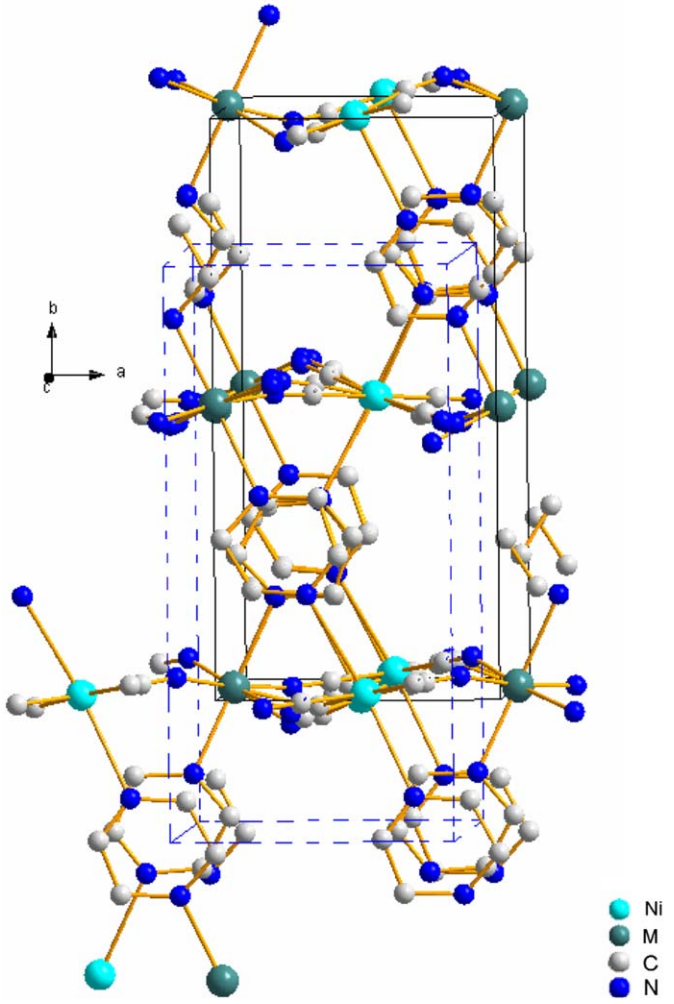

Fig. 4. Atomic packing within the unit cell for the high (continuous line) and low (discontinuous line) temperature phases for Mn, Co, Zn and Cd.

3.3. Crystal structures for the low temperature phases

The crystal structures for the low temperature phases were solved from *ab initio* using the Patterson methods and then refined by the Rietveld method, for $T[Ni(CN)_4]\cdot 2pyz$ with T=Mn, Co, Zn, Cd, and $Ni[Ni(CN)_4]\cdot pyz$ in the *Pc* and *P*4/*m* space groups, respectively. As already mentioned, for Ni the low and high temperature phases have the same symmetry properties (*P*4/*m* space group).

For Mn, Co, Zn and Cd the atomic coordinates for the low and high temperature phases, monoclinic and orthorhombic, respectively, were found to be related according to: $x'=x+0.1667$; $y'=y+0.25$; $z'=z$. During the crystal structure refinement the allowed variations for Ni–C and C–N interatomic distances and C–Ni–C and Ni–C–N bond angles, were restricted to be within certain intervals. These atoms remain linked through triple bonds with expected small variations for the bond distances. By the same reason, for the Ni–C–N chain no large deviation from the linearity is expected. For T=Zn and Ni in Table 3 the refined atomic positions and thermal and occupation factors are summarized, and in Table 4 the calculated bond distances and angles are given. For the remaining compositions the refinement results are available from Supplementary information.

Fig. 4 shows the atomic packing within the unit cell for the monoclinic phase. The structural motifs for the high and low temperature phases are different. The low temperature modification preserves the main features of the parent room temperature structure. In both structural models, the Ni and T metals are found with a pseudo-octahedral coordination, $Ni(C_4)_{CN}(N_2)_{pyz}$ and $T(N_4)_{CN}(N_2)_{pyz}$, respectively. All the pyrazine molecules are forming bridges between Ni and T metals in the interlayers region, Ni–pyrazine–T. Along the **c** axis, the pyrazine molecules are found stacked according to a crossed configuration. However, unlike to the orthorhombic model, the monoclinic structure contains two structural sites for the pyrazine molecule with slightly different interaction with the T metal and, in consequence, with also different T-pyrazine bond distances (see Table 4). This results in certain distortion for the $T(N_4)_{CN}(N_2)_{pyz}$ octahedron, and into the appearance of two different interlayer distances, 7.91 and 7.69 Å, along the **b** unit cell axis. For the T–NC distance also slight changes were observed. These small variations for the T–N distances result in the above indicated unit cell volume reduction on the structural transformation. Additional details on these small structural changes are available from the Supplementary information file.

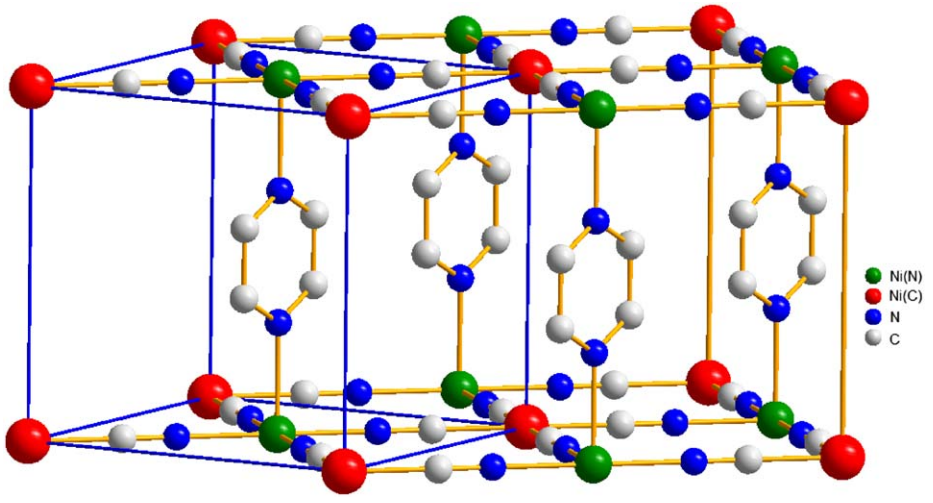

Fig. 5. Atomic packing within the unit cell for the high (left cell, Z=1) and low (right cell, Z=2) temperature phases of $T[Ni(CN)_4]\cdot pyz$ with T=Co, Ni.

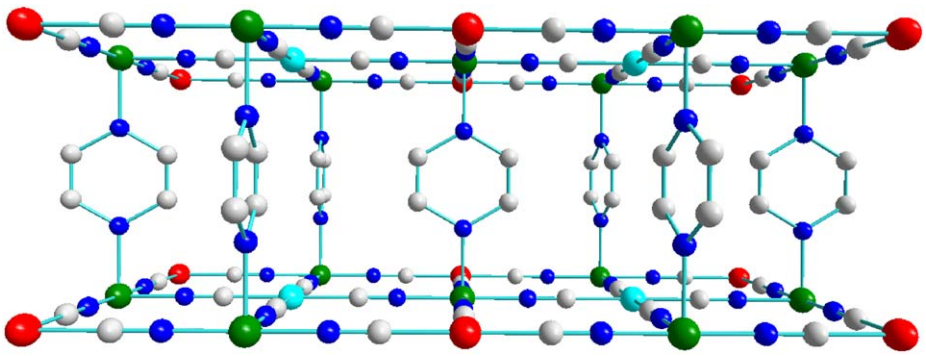

Fig. 6. Atomic packing within the framework for the low temperature phase of $T[Ni(CN)_4]\cdot pyz$ with T=Co, Ni. Due to the observed ordered configuration (non-rotating) for the pyrazine molecules, the unit cell contains two structural sites for the Ni atom linked at the C end of the CN group.

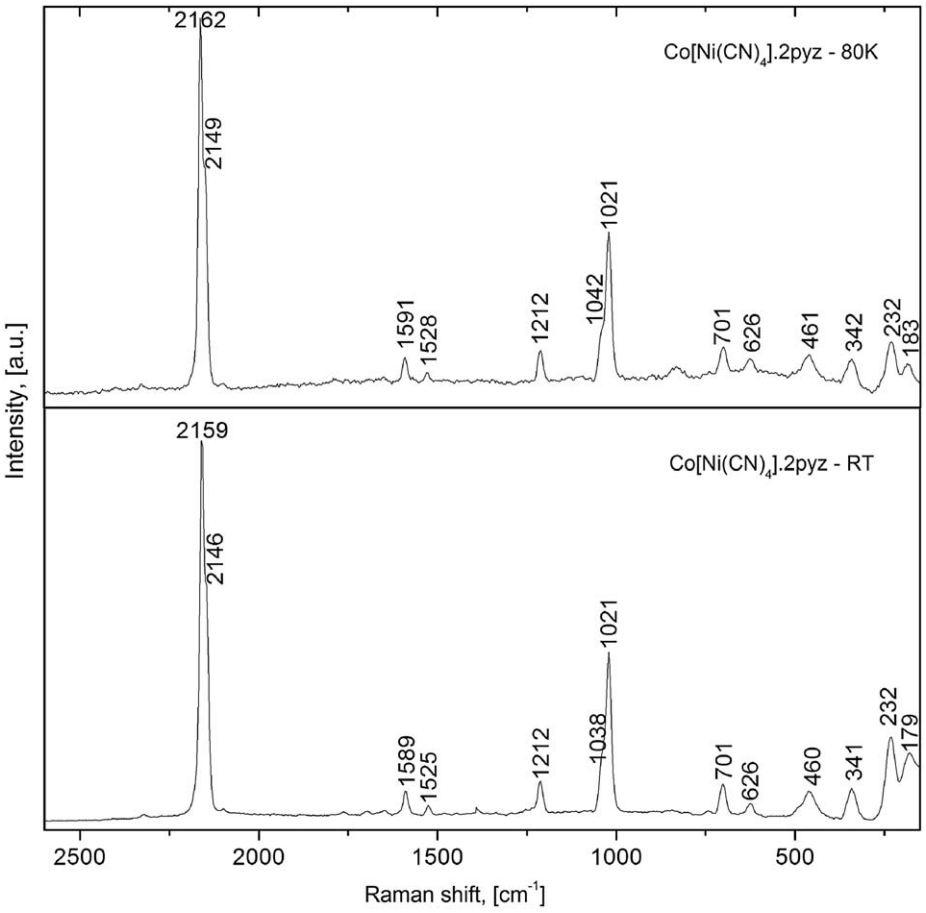

Fig. 7. Raman spectra for the low (monoclinic) and high (orthorhombic) temperature phases of $Co[Ni(CN)_4]\cdot 2pyz$.

The low temperature phase for the mono-pyrazine Ni compound contains two formula units per unit cell (Z=2), versus Z=1 for the high temperature phase (Fig. 5). Such size increase for the minimum repetitive block within the material framework is related to the appearance of two different structural sites for the Ni atom linked at the C end of the CN group. This structural change was ascribed to the pyrazine molecules environment. While in the tetragonal high temperature structure all the pyrazine molecules remain rotating around its axis and are equivalent, in the low temperature modification the pyrazine molecules were found to be non-rotating, adopting an ordered structure (Fig. 6). For such configuration of pyrazine molecules the maximum distance between their electron clouds and the minimum electrostatic repulsive energy between them correspond. The refined atomic positions and thermal and occupation factors are collected in Table 3. The calculated bond distances and angles are given in Table 4. The ordered configuration for the pyrazine molecules related to the minimum value for the repulsive energy also explains the observed changes for equatorial Ni–NC and axial Ni–N_{pyz} bond distances, from 2.153 and 2.038 Å (room temperature) to 1.926 and 2.060 Å (77 K), respectively. These changes for the bond distances are supported by the recorded Raman spectra. The HR-XRD patterns recorded at 12 K were of insufficient quality

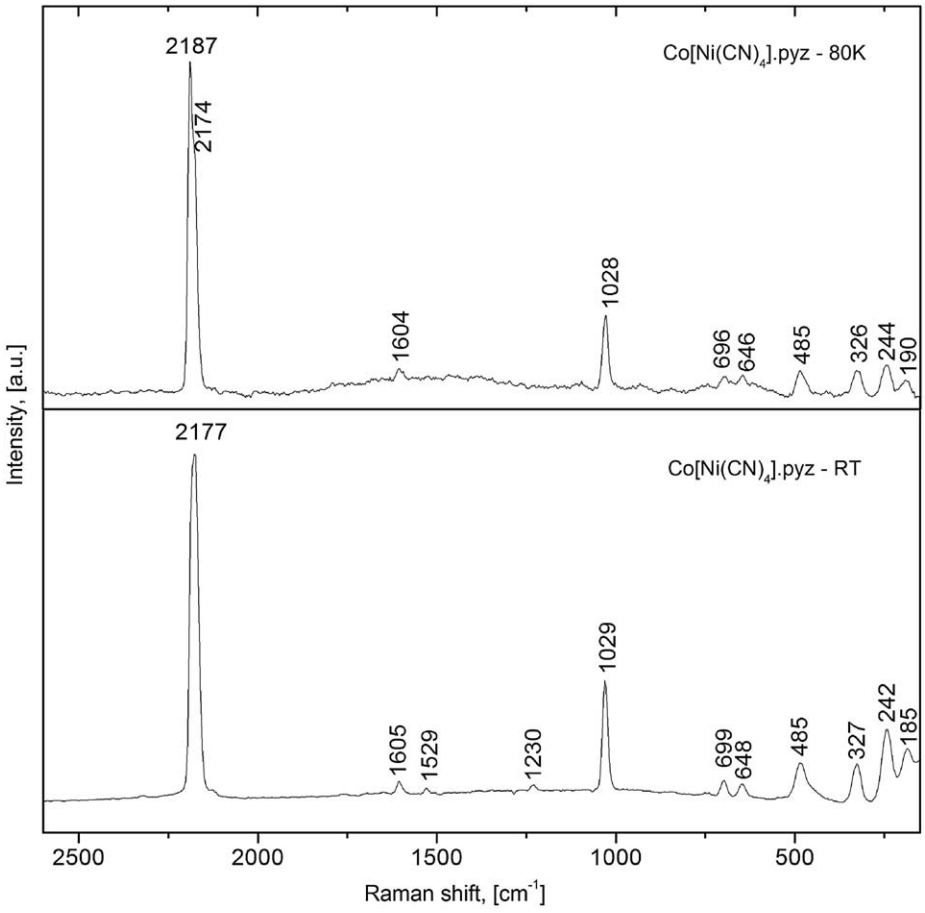

Fig. 8. Raman spectra for the low and high temperature tetragonal phases of $Co[Ni(CN)_4]\cdot pyz$.

Table 5
The Raman vibrations observed for the high and low temperature phases of $Co[Ni(CN)_4]\cdot xpyz$.

	CoNi2pyz-RT	CoNi2pyz-80K	CoNipyz-RT	CoNipyz-80K
ν(CN)	2159	2162	2177[a]	2187
	2146	2149		2174
ν_{ring}	1589	1591	1605	1604
	1525	1528	1529	[b]
δ(CH)	1212	1212	1230	[b]
ν_{ring}	1021	1021	1029	1028
δ_{ring}	701	701	699	696
	626	626	648	646
γ_{ring}	460	461	485	485
ν(Co–N_{pyz})	341	342	327	326
$N_{(pyz)}$–Ni	232	232	242	244
ν(Co–N_{CN})	179	183	185	190

[a] Only a broad peak is observed.
[b] Not observed.

(low statistic) to be used for the structure refinement. These patterns were collected in order to explore the possibility of an additional phase transition on cooling below 77 K.

3.4. Related changes for the electronic structure

Figs. 7 and 8 show the recorded Raman spectra at room temperature and at 80 K for $Co[Ni(CN)_4]\cdot xpyz$ with x=1, 2. In Table 5 the assignment of the observed vibrations is reported. The Raman spectroscopy data for the remaining compositions are available from Supplementary information. The frequency for the ν(CN) vibration is an excellent sensor for the electronic structure of cyanometallates because it senses the changes that take place at both N and C ends. The ground-state electronic structure for the CN ligand is $(1\sigma)^2(2\sigma)^2(3\sigma)^2(4\sigma)^2(1\pi)^4(5\sigma)^2$. The highest lone pair (5σ) is mainly involved in the M–CN bond but also in the more ionic CN–T interaction. The CN group has two extended π^*-antibonding orbitals at C end of relatively low energy able to interact with the metal (M) t_{2g} orbitals. During the tetracyanide complex formation, $[M(CN)_4]^{2-}$, the CN group participates of a particularly strong donating interaction with the metal, and all the *nd* electrons of this last one are forced to occupy its b_{2g} (xy), e_g (xz,yz) and $a_{1g}(z^2)$ orbitals. Such large electron density on the metal induces certain electron back-donation into the ligand π^*-orbitals. The charge removed from the inner metal (M) is mainly localized on the N end and partially donated to the metal T during the complex metal salt formation. All these interactions produce slight variations within the C≡N bond and it is sensed by the ν(CN) frequency. For $T[Ni(CN)_4]\cdot 2pyz$ the structural transformation is accompanied of a positive shift of about $3\,cm^{-1}$ for the frequency of this vibration. This agrees with the observed shit of $+4\,cm^{-1}$ for the $\nu(T\text{–}N_{CN})$ vibration, and is interpreted as an enhancement for the T–N_{CN} interaction. Since no appreciable shifts are observed for characteristic internal pyrazine vibrations, the metal is subtracting a higher amount of charge from the ligand 5σ orbital, which has a slight anti-bonding character, and this is sensed by the observed positive shifts in frequency for the ν(CN) and $\nu(T\text{–}N_{CN})$ vibrations. For the

tetragonal phase the frequency shift for these two vibrations is even higher (Table 5), corresponding to a stronger T–N_{CN} interaction in the low temperature phase. It seems the ordered structure for the pyrazine molecules leads to a weaker repulsive interaction also with the metal t_{2g} electrons and this favors a higher CN→T charge donation. All these changes detected from the Raman spectra support the refined crystal structures.

4. Conclusions

On cooling in both orthorhombic and tetragonal phases of transition metal tetracyanonickellates pillared with pyrazine molecules a structural transformation is detected. For the orthorhombic structure, $T[Ni(CN)_4]\cdot 2pyz$, about 185 K a monoclinic phase is formed. In $T[Ni(CN)_4]\cdot pyz$ (tetragonal phase) the change is detected about 120 K and it is related to the appearance of an ordered state for the pyrazine molecules. Above this temperature all the pyrazine molecules are found rotating. These low temperature structural changes are accompanied of an enhancement for the T–N_{CN} interaction. The low temperature phases correspond to a stronger T–N_{CN} bond. The HR-XRD structural results are supported by the information obtained from low temperature calorimetric measurements and Raman spectra.

Supplementary information

Structural information derived from the crystal structures refinement for the low temperature phase of the studied materials has also been deposited at the Cambridge Crystallographic Data Centre (e-mail: deposit@ccdc.cam.ac.uk) with CCDC file numbers: CCDC 732243: $Mn[Ni(CN)_4]\cdot 2pyz\_77K$; CCDC 732242: $Zn[Ni(CN)_4]\cdot 2pyz\_77K$; CCDC 732244: $Cd[Ni(CN)_4]\cdot 2pyz\_77K$; CCDC 732245: $Ni[Ni(CN)_4]\cdot pyz$; CCDC 732246: $Ni[Ni(CN)_4]\cdot pyz\_77K$; CCDC 733492: $Co[Ni(CN)_4]\cdot 2pyz$ and CCDC 733491: $Co[Ni(CN)_4]\cdot 2pyz\_77K$.

Acknowledgments

A.A.L.-S acknowledges the support provided by CONACyT (Mexico) and UNAM Environmental Nanotechnology Project (PUNTA) for her PhD studies. The help of M. Avila-Santos for HR-XRD data collection and of F. Rodríguez-Melgarejo for the Raman spectra acquisition is highly appreciated. This research was partially supported by the Projects SEP-CONACyT-2007-61-541 and ICyTDF-PIFUTP08-158. Access to the LNLS synchrotron radiation facility (at Campinas, Brazil) is also acknowledged.

Appendix A. Supplementary material

Supplementary data associated with this article can be found in the online version at doi:10.1016/j.jssc.2009.11.004.

References

[1] Y. Li, Y. Liu, Y. Wang, Y. Leng, L. Xie, X. Li, Int. J. Hydrog. Energy 32 (2007) 3411.
[2] J.T. Culp, S. Natesakhawat, M.R. Smith, E. Bittner, C. Matranga, B. Bockrath, J. Phys. Chem. C 112 (2008) 7079.
[3] T. Kitazawa, Y. Gomi, M. Takahashi, M. Takeda, M. Enomoto, A. Miyazaki, T. Enoki, J. Mater. Chem. 6 (1996) 119.
[4] V. Niel, J.M. Martínez-Agudo, M.C. Muñoz, A.B. Gaspar, J-A. Real, Inorg. Chem. 40 (2001) 3838.
[5] G. Molnár, V. Niel, A.B. Gaspar, J-A. Real, A. Zwick, A. Bousseksou, J.J. McGarvey, J. Phys. Chem. B 106 (2002) 9701.
[6] G. Molnár, V. Niel, J-A. Real, L. Dubrovisnky, A. Bousseksou, J.J. McGarvey, J. Phys. Chem. B 107 (2003) 3149.
[7] G. Molnár, T. Kitazawa, L. Dubrovisnky, J.J. McGarvey, A. Bousseksou, J. Phys. Condens. Matter 16 (2004) S1129.
[8] T. Tayagaki, A. Galet, G. Molnár, M.C. Muñoz, K. Tanaka, J-A. Real, A. Bousseksou, J. Phys. Chem. B 109 (2005) 14859.
[9] S. Cobo, D. Ostrovskii, S. Bonhommeau, L. Vandier, G. Molnár, L. Salmon, K. Tanaka, A. Bousseksou, Am. Chem. Soc. 130 (2008) 9019.
[10] G. Agustí, S. Cobo, A.B. Gaspar, G. Molnár, N.O. Moussa, P.A. Szilágyi, V. Pálfi, C. Vieu, M.C. Muñoz, J.-A. Real, A. Bousseksou, Chem. Mater. 20 (2008) 6721.
[11] A.A. Lemus-Santana, J. Rodriguez-Hernandez, L.F. Del Castillo, M. Basterrechea, E. Reguera, J. Solid State Chem. 182 (2009) 757.
[12] G.M. Sheldrick, Program for Crystal Structure Determination, Institut für Anorg. Chemie, Göttingen, Germany, 1997.
[13] A.L. Le Bail, ESPOIR: a program for solving structures by Monte Carlo from powder diffraction data, in EPDIC-7, Barcelona, 2000, 〈http://www.cristal.org/sdpd/espoir/S〉.
[14] J. Rodríguez-Carvajal, FullProf 2005 Program, Institute Louis Brillouin, Saclay, France, 2005.